Biophysical mechanisms to relate large-scale brain network dynamics to individual-specific variability of perception

G. Vinodh Kumar*, Shrey Dutta*, Siddharth Talwar, Dipanjan Roy§, Arpan Banerjee§

Cognitive Brain Dynamics Lab, National Brain Research Centre,

NH-8, Manesar, Gurgaon-122052, Haryana, India

* Authors have equal contribution

§ Joint corresponding authors: dipanjan.nbrc@gov.in (Dr. Dipanjan Roy); arpan@nbrc.ac.in (Dr. Arpan Banerjee)

Abstract

Perception necessitates interaction amongst neuronal ensembles, the dynamics of which can be conceptualized as the emergent behavior of coupled dynamical systems. Likewise, the variability in perception can be explained to emerge from the modulation of interactions within the underlying neural dynamical system. Employing this framework, we explain the inter-individual variability in McGurk effect – wherein illusory sound is perceived when presented with certain semantically-incongruent audio-visual (AV) syllables. We computed global coherence to capture the cortical dynamics in the electroencephalogram (EEG) signals while the participants with varying McGurk susceptibility perceived congruent and incongruent McGurk-AV syllables. We observed that McGurk susceptibility was negatively correlated to participants' alpha band global coherence. Our neurobiologically-realistic dynamical model attributed the decrease in alpha band coherence to extremely weak direct auditory(A)-visual(V) coupling that were then validated by source connectivity analysis among constituent cortical generators of neural activity. Overall, we provide a link between functional metrics and underlying neurophysiological mechanisms.

Introduction

Neurobiologically realistic dynamical models of perception have provided attractive explanation of behavior (Moreno-Bote et al 2007, Thakur et al., 2016; Cuppini et al., 2017) . Concurrently, they also provide insights to brain dynamics observed at different scales e.g., microscopic level of single neurons (Deco et al., 2007; Lim et al., 2011) and macroscopic level of field recordings (David & Friston, 2003; Spiegler et al., 2011; Onojima et al., 2018). How does this framework adapt to the subjective nature of perceptual variability across individuals during the perception of complex signals? One intuitive approach to explain perceptual variability involves characterization of noise in component neural systems. Thereafter, probability distributions set by internal processes that generate prediction can follow Bayes' optimization principles to set up perceptual object identification (Körding et al., 2007; Ma et al., 2008). One drawback of such models is that they miss neurobiological mechanisms and systems-level interactions that govern perception (Magosso et al., 2012; Ursino et al., 2017). In this article, we use the old workhorse of multisensory speech perception: McGurk effect (McGurk & Macdonald, 1976) to demonstrate how the systems-level interactions in multisensory and unisensory subsystems can explain differences in McGurk susceptibility across individuals.

The fact that speech perception is fundamentally driven by visual cues is demonstrated in this paradigm - an auditory /*ba*/ dubbed onto visual lip movements of /*ga*/ is perceived by the listener as a completely different syllable /*da*/ (McGurk & Macdonald, 1976). Variability in the perception of the illusion has provided researchers a practical advantage to study and unravel the neural correlates of illusory/cross-modal percept in terms of cortical activations and neural oscillations (Beauchamp, 2010; Nath & Beauchamp, 2011; Keil et al., 2012). However, until recently, studies have overlooked the substantial variability of McGurk susceptibility across individuals that could influence the objective behavioral and neural estimates.

From a neurophysiological standpoint, how do we reconcile the neural correlates of McGurk percept under the purview of inter-individual variability or vice versa? Moreover, it raises a fundamental question on what constitutes an appropriate neural correlate. For instance, activity in superior temporal sulcus (STS) and its functional connectedness to sensory specific and fronto-parietal regions has been shown to subserve multisensory speech perception (Beauchamp, 2010; Nath & Beauchamp, 2011; Keil et al., 2012) and McGurk susceptibility (Nath &

Beauchamp, 2012) as well. Moreover, other research areas like face processing (Haxby et al., 2000), motion perception (Puce & Perrett, 2003) and social perception (Saxe, 2006) attribute the elicitation of their behavior of interest to activations in STS. Put together, these findings make STS only a prime nexus of information processing, not a neural correlate for a specific behavioral trait.

Contrary to the traditional approach of pinning down on a putative brain area, substantial body of emerging studies indicate complex cognitive capabilities to emerge as a result of interactions amongst large-scale networks of cortical areas (Bressler, 1995; Bressler & Kelso, 2001; Bressler & Menon, 2010; Varela et al., 2001). Therefore, a measure that could capture the 'dynamic' and 'preferential' interactions amongst distributed neuronal assemblies/brain regions will offer the most pertinent representation of the distinct neural machinery supporting McGurk susceptibility.

Recent studies have indicated that beyond a specific region of interest, a large-scale network of oscillatory brain networks are involved in effectuating McGurk percept (Kumar et al., 2016; Kumar et al., 2017). A key question emerges, how robust is this network across individuals and whether the organization of such networks is contingent on the stimulus configurations. Secondly, what are the neural mechanisms that give rise to such network level correlates? While the first question needs to be answered empirically using a detailed neurophysiological study of underlying brain networks, the more broader question of systems-level insight require a neurobiologically inspired large-scale computational model.

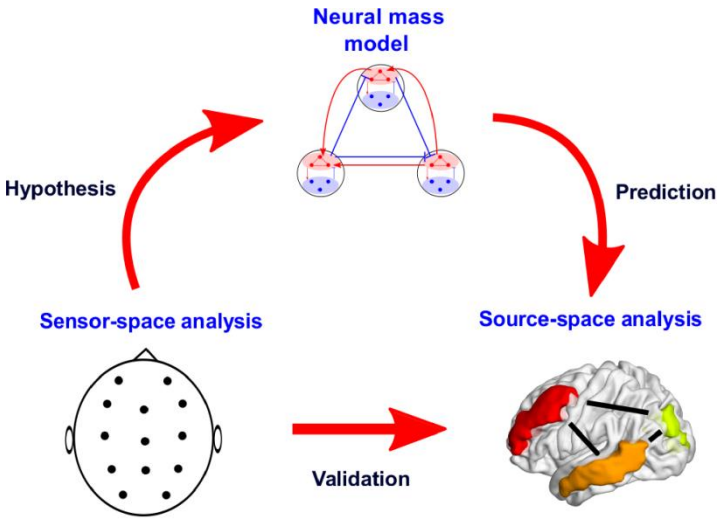

Figure 1 Pipeline of the study**:** We address an ongoing challenge of characterizing the neural mechanisms that govern the variability during multisensory speech perception. Employing the McGurk paradigm, we identify the neural signatures of the variability in the global coherence metric. We then turn to test our hypothesis – 'dynamic and preferential coupling between sensory specific and multisensory regions underlie the observed variability', using a neural mass model. Finally, we validate the inferences drawn from the model by analyzing pairwise coherence in the source space between concordant cortical generators of neural activity.

We hypothesized that variability in McGurk susceptibility across individuals stem from implicit differences in their large–scale functional connectivity. In order to test our hypothesis; we conducted psychophysical experiments in tandem with EEG recordings to characterize the large-scale oscillatory modes in whole-brain dynamics. Subsequently we conceptualized a neural mass model for multisensory perception - an abstraction of summed synapto-dendritic activity of thousands of neurons, comprising three nodes representing sensory and multisensory areas. Finally, we validated the plausible neural mechanisms made by the model using source space analysis (**Figure 1**), thus providing a link between functional metrics and underlying neurophysiological complexity.

Results

Variability in multisensory perception

Incongruent McGurk stimulus, visual /*ka*/ paired with audio /*pa*/, and three kinds of congruent AV stimuli - /*ta*/, /*pa*/, /*ka*/ were presented to all participants. The sequence of presentation was randomized. As the participants observed each of the stimulus, they were instructed to report with a set of four keys if they heard /*ta*/, /*pa*/, /*ka*/ or 'something else'. A high degree of *inter-individual* variability in McGurk susceptibility was observed (**Figure 2A**). Subsequently, the participants were classified based on their McGurk susceptibility in the incongruent trials into two groups – rare perceivers (<50% /*ta*/ percept) and frequent perceivers (>50% /*ta*/ percept). Eight of the eighteen participants elicited <50% propensity of perceiving the McGurk effect.

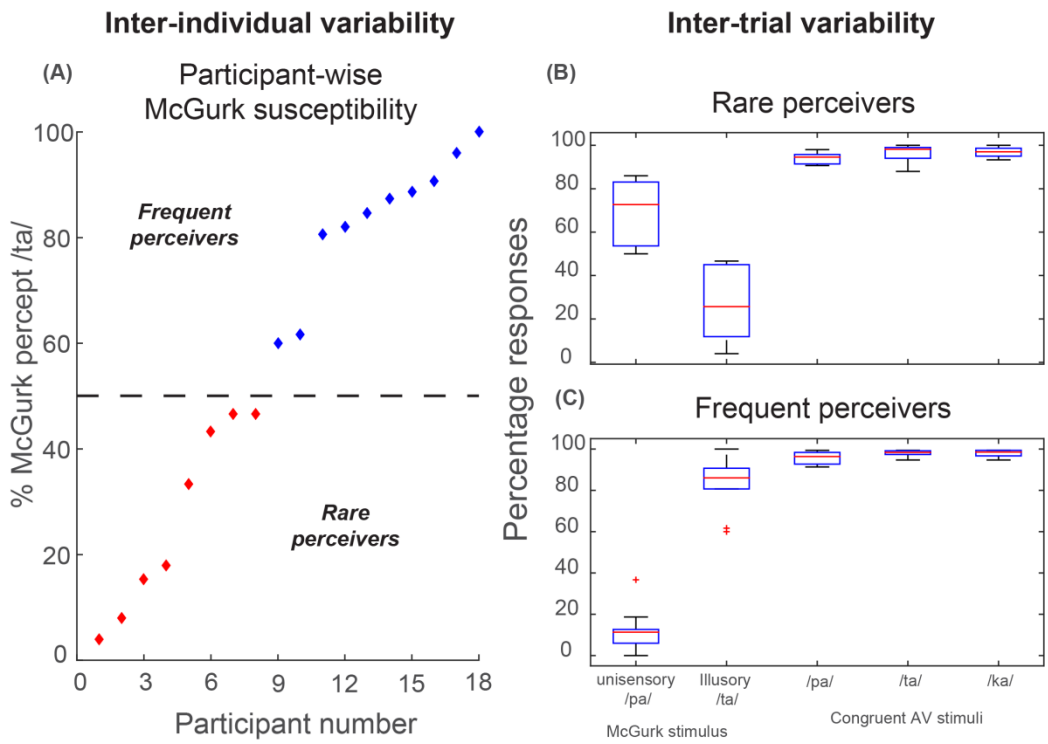

Figure 2 Behavior: (A) *Inter-individual variability* - Propensity of McGurk effect for each of the 18 participants expressed as the percentage of /*ta*/ percept during the presentation of McGurk stimulus. The participants were categorized as frequent perceivers (blue diamonds, >50%) and rare perceivers (red diamonds, <=50%). *Inter-trial variability* - Percentage of /*ta*/ (illusory) and /*pa*/ (unisensory) percept during the presentation of McGurk stimulus and the hit rate during the presentation of congruent AV stimuli (/*pa*/, /*ta*/ and /*ka*/) averaged over (B) Rare perceivers (C) Frequent perceivers

Response tendency (*inter-trial variability*), computed as the relative proportion of illusory (/*ta*/) responses in all McGurk trials across all participants in each group (rare and frequent perceivers) explicitly, showed that rare perceivers reported /*ta*/ percept in 26.96% (SD = 17.63) of trials, whereas unisensory /*pa*/ percept was reported in 69.35% (SD = 15.65) trials (**Figure 2B**). However, frequent perceivers reported /*ta*/ percept in 83.17% (SD =13.16) trials, whereas unisensory /*pa*/ percept was reported in 12.13% (SD = 10.09) trials (**Figure 2C**). The difference between the mean of /*ta*/ and /*pa*/ percepts during McGurk stimulus were significantly different in both rare (t_{14} = -5.08, p < 0.001) and frequent perceivers (t_{18} = 13.54, p <0.001). Congruent AV stimuli (/*ta*/, /*pa*/ and /*ka*/) were correctly identified in 95.72% (SD = 3.30) and 97.22% (SD = 2.32) trials by rare and frequent perceivers respectively (**Figure 2B, C**). We ran one-way ANOVA on the percentage of correct responses during congruent AV stimuli: /*pa*/, /*ta*/ and /*ka*/. We observed no significant difference between the percentage responses between the three congruent stimuli both in rare, $F(2,23)=1.75$, $p=0.19$ and frequent $F(2,29=2.91$, $p=0.07$ perceivers.

Large-scale functional connectivity in EEG sensor space

The emergence of specific cognitive trait is subserved by the coordination of distributed functionally specialized neuronal assemblies or brain regions (Bressler, 1995; Varela et al., 2001; Bressler & Menon, 2010). Based on our previous study (Kumar et al., 2016), we hypothesized that neural signatures of inter-individual and inter-trial variability can be quantified using the global coherence metric that capture the degree of neuronal synchronization over the entire brain from EEG scalp-level recordings.

Global coherence differences between rare and frequent perceivers (between-group) were examined using cluster based permutation tests in specific frequency bands: theta (4-8 Hz), alpha (9-14 Hz), beta (15-30 Hz) and gamma (31-45 Hz). Significant increase in global coherence in theta, alpha and beta bands were observed in rare perceivers (see Table 1 for details). However, their global coherence in gamma band was significantly lower than frequent perceivers (**Figure 3A-D**).

Table 1: Percentage increase in the coherence and the quantile (5th and 95th) values of the test statistic during cluster based permutation tests.

Stimuli	**Frequency bands**			
	Theta (4-8Hz)	*Alpha (8-14Hz)*	*Beta (15-30 Hz)*	*Gamma (31-45 Hz)*
Incongruent McGurk	2.60% $z_{95} = 0.19$	7.69% $z_{95} = 0.26$	14.83% $z_{95} = 0.16$	4.37% ($z_{0.05} = -0.17$)
Congruent /pa/	3.10% $z_{95} = 0.18$	6.63% $z_{95} = 0.26$	11.25% $z_{95} = 0.17$	7.18% ($z_{0.05} = -0.18$)
Congruent /ta/	6.06% $z_{95} = 0.18$	5.64% $z_{95} = 0.25$	12.00% $z_{95} = 0.15$	7.45% ($z_{0.05} = -0.17$)
Congruent /ka/	6.78% $z_{95} = 0.19$	12.68% $z_{95} = 0.26$	14.99% $z_{95} = 0.15$	9.51% $z_{0.05} = -0.17$

Next, global coherence in the aforementioned bands were investigated vis-à-vis McGurk susceptibility in individual participants. Spearman rank correlation showed the existence of a significant negative correlation at 95% significance between alpha band global coherence and the McGurk susceptibility during incongruent McGurk ($r_s(18)$ =-0.49, p=0.04) (**Figure 3E**), congruent /*ta*/ ($r_s(18)$ =-0.51, p=0.03) (**Figure 3G**) and /*ka*/ ($r_s(18)$ =-0.49, p=0.04) (**Figure 3H**) AV stimuli. However, during congruent /*pa*/ AV stimuli, no correlation was observed between alpha band global coherence and McGurk susceptibility ($r_s(18)$ =-0.18, p=0.47) (**Figure 3F**). Evidently, there were also no correlation between global coherence in any other frequency band and McGurk susceptibility during McGurk , theta: $r_s(18)$ =-0.29, p=0.22., beta: $r_s(18)$ =-0.21, p=0.39, gamma: $r_s(18)$ =-0.49, p=0.04; congruent /*pa*/, theta: $r_s(18)$ =-0.38, p=0.12, beta: $r_s(18)$ =-0.14, p=0.57, gamma: $r_s(18)$ =-0.15, p=0.53; congruent /*ta*/ theta: $r_s(18)$ =-0.36, p=0.14, beta: $r_s(18)$ =-0.17, p=0.50, gamma: $r_s(18)$ =-0.19, p=0.42, and congruent /*ka*/ (theta: $r_s(18)$ =-0.31, p=0.20, beta: $r_s(18)$ =-0.22, p=0.37, gamma: $r_s(18)$ = -0.16, p=0.50 stimuli.

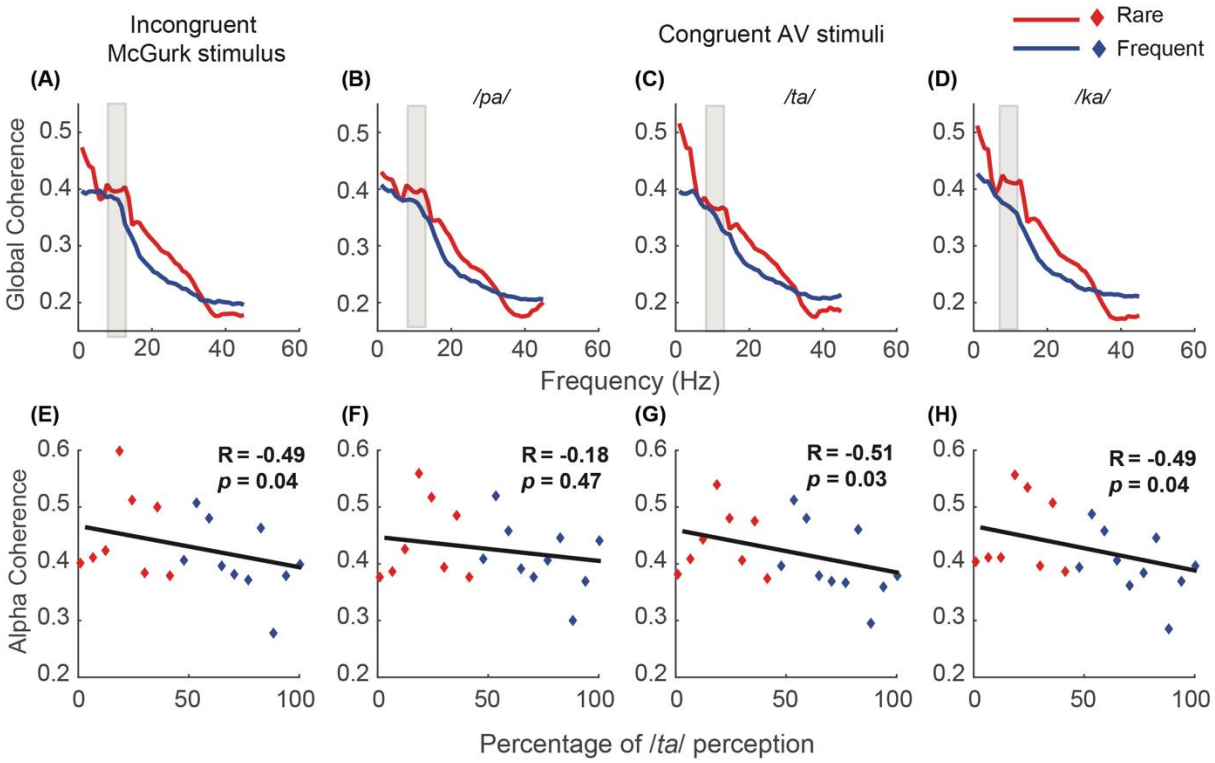

Figure 3 Large scale functional connectivity: *Inter-individual variability* – Time averaged global coherence during stimulus: (A) incongruent McGurk (B) Congruent /*pa*/ (C) Congruent /*ta*/ (D) Congruent /*ka*/. The shaded region represents the global coherence in the alpha band that was averaged and used for correlation analysis. Mean alpha band coherence plotted against participants susceptibility of McGurk effect during stimulus: (E) McGurk (F) Congruent /*pa*/ (G) Congruent /*ta*/ (H) Congruent /*ka*/.

A simple interacting neural mass model with fast, intermediate and slow time-constants explains desynchronization of alpha band global coherence

Global coherence dynamics may reflect the potential operation of a large-scale network that support multisensory speech perception. We hypothesized that the variability in McGurk percept across participants to be grounded in specific interactions between neural assemblies (**Figure 4**). In order to account for the observed global coherence patterns, we employed a neural mass model comprising three nodes broadly representing the auditory and visual areas in the sensory cortices, and the multisensory node representing the collection of multisensory (modality-nonspecific) areas. Each node comprised a population of excitatory and inhibitory Hindmarsh-Rose (HR) neurons (Hindmarsh & Rose, 1984) operating at different physiologically motivated time-scales (see Materials and Methods for more details).

We sought to explore the global coherence while varying the configuration and strength of coupling among the nodes in our model. For instance, in **figure 4A** auditory node's excitatory coupling of $+W_{AV}$ on multisensory node was balanced with inhibitory coupling of the same strength ($-W_{AV}$) from the multisensory node. In such a configuration, auditory node is being the source of excitation, is referred as the source whereas multisensory node is referred as the sink since all excitatory couplings are directed towards it. The visual node in such configuration behaves as both source and sink.

The co-existence of coherence in alpha and gamma band facilitated by the two time scales of visual (slow) and auditory (fast) node was observed in network configuration wherein visual node operates as the source and auditory node acts as a sink (**Figure 4G**). Moreover, the concurrence of the coherence in alpha and gamma bands emerged in the coupling between auditory and visual regions (coupling parameter ranging between 0.35 and 0.7) via two routes – 1) direct coupling (W_{AV}) and 2) indirect coupling (W_{AM} & W_{VM}) involving multisensory node (M). We assumed coupling strength less than 0.35 to be weak coupling (WC), coupling strength between 0.35 and 0.7 to be moderate coupling (MC) and coupling greater than 0.7 to be strong coupling (SC). In SC range, we observed high coherence in alpha band and gamma bands, however, no peak was observed in alpha band. In the MC range, none of the model configurations were able to generate concurrent coherent states in alpha and gamma bands (**Figure 4A-H**), except **Figure 4G,** where visual node acts as the source of excitation. Furthermore, direct coupling between auditory and visual node alone (W_{AV} ranges from 0 to 1, W_{AM} & W_{VM} = 0) results only in alpha band coherence (**Figure 4J**). Interestingly, emergence of only gamma band coherence was observed when the indirect coupling in the model were varied between A-V nodes via multisensory node (W_{AM} & W_{VM} range from 0 to 1, W_{AV} = 0) in MC range (**Figure 4K**).

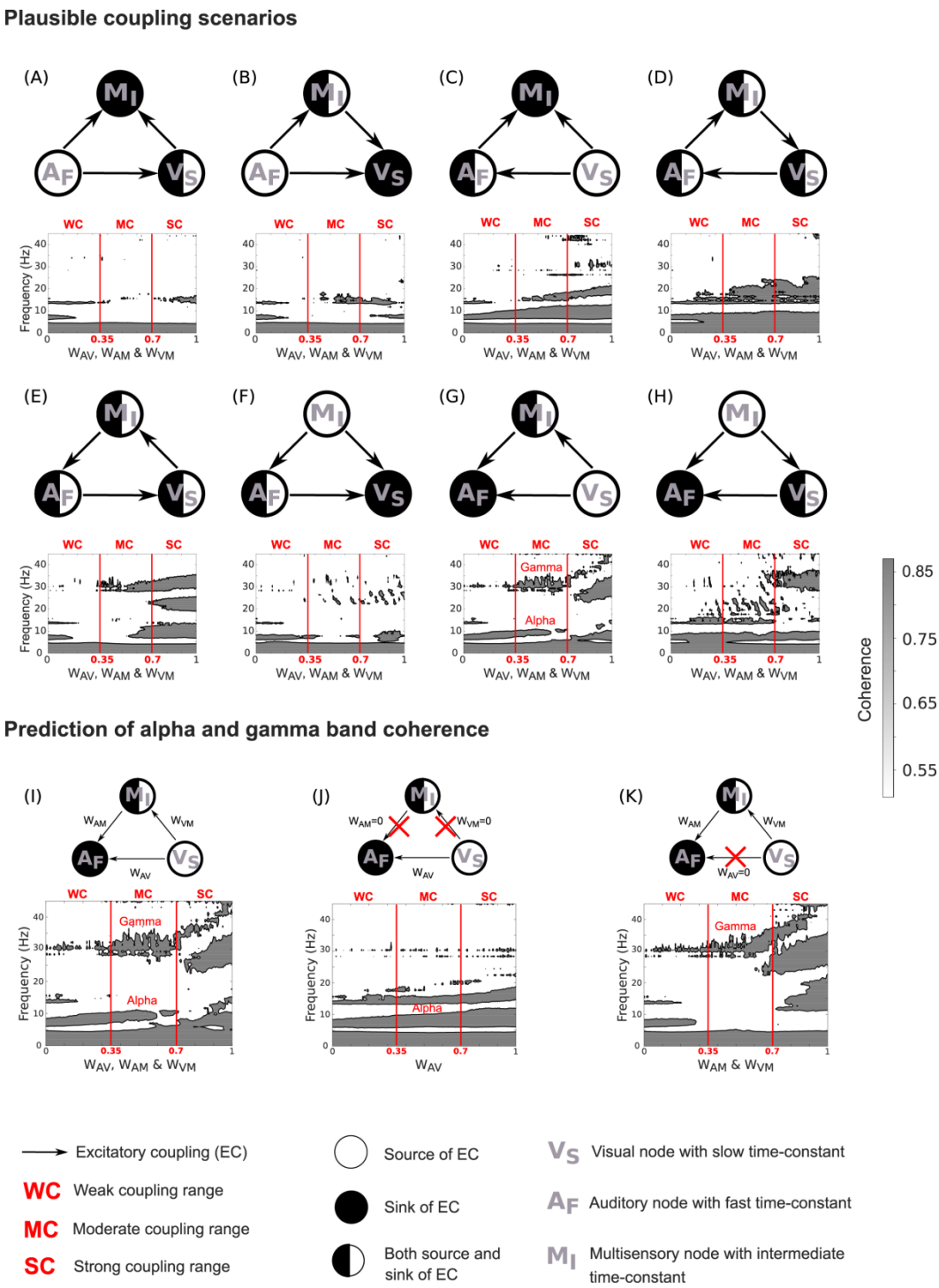

Figure 4 Prediction of alpha and gamma coherences from neural mass model: (A) - (H) Exploration of various coupling scenarios to identify if it is possible to generate alpha and gamma coherence in moderate coupling range. Only the model configuration (G) exhibits concurrent coherence in the alpha and gamma band in the moderate coupling range. I) Alpha and gamma band coherences co-exist in moderate coupling range when visual node is source and auditory node is the sink J) Only direct A-V coupling generates alpha coherence independently. K) Indirect A-V coupling via multisensory node generates gamma coherence at the limit case scenario of weak direct coupling.

Direct Audio-Visual interaction underpins Inter-Individual Variability

Our empirical findings indicate a significant negative correlation between participant-wise alpha band coherence and McGurk susceptibility. Rare perceivers were characterized by enhanced alpha band coherence than frequent perceivers. We hypothesized that mediation of interaction between auditory (A) and visual (V) node via the multisensory node (M) (i.e. stronger A-M and V-M coupling than A-V coupling) to be characteristic of participants with higher susceptibility to the McGurk effect. To test this hypothesis, a balanced network coupling state, $W_{AM} = W_{VM} = W_{AV} = 0.35$ where alpha and gamma band coherences co-exist was considered, following which the change in the coherence peaks with decreasing direct A-V coupling (W_{AV}) was studied. A suppression of alpha coherence peak with decrease in W_{AV} was observed (**Figure 5**); however, gamma coherence peak remained more or less unchanged. Only when A-V coupling in the computational model became negligible ($W_{AV} < 0.05$), disappearance of alpha coherence peak was observed.

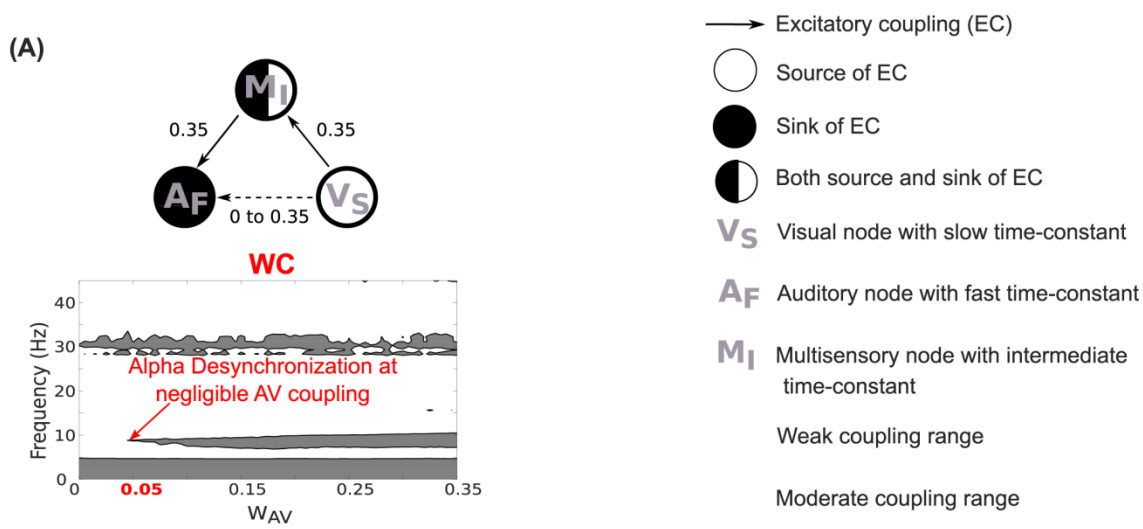

Figure 5 Mechanistic understanding of Inter-individual variability:
A) Alpha de-synchronization characteristic of frequent perceivers resulted due to negligible A-V coupling.

Validation of model predictions using source-connectivity analysis

Finally, we obtained source level time series for each brain parcel by projecting single trial time series to the source-space by multiplying them with spatial filter of the respective parcel using voxel to parcel mapping provided by AAL atlas (see materials and methods for details). Subsequently, the pairwise coherence - a measure of functional connectedness, between the parcels associated with auditory and visual areas were computed. Auditory specific parcel – Superior Temporal Gyrus (STG) and the visual parcels – Superior Occipital Cortex (SOC), Medial Occipital Cortex (MOC) and Inferior Occipital Cortex (IOC) were identified. Significantly increased functional connectivity between left STG- left SOC ($t(998)=171.59$, $p<0.0001$) (**Figure 6A**) and left STG- left MOC ($t(998)=130.94$, $p<0.0001$) (**Figure 6C**) was observed in rare perceivers compared to frequent perceivers suggesting accuracy of the model based predictions that rare perceivers possess stronger connectivity between auditory and visual nodes. However, there was no significant difference in the connectivity between left STG-left IOC ($t(998)=-45.05$, $p=0.14$) (**Figure 6E**). Also, there was no significant difference in the connectivity between right STG- right SOC ($t(998)=-25.66$, $p=0.61$) (**Figure 6B**), right STG-right MOC ($t(998)=32.94$, $p=0.12$) (**Figure 6D**), right STG- right IOC ($t(998)=-81.39$, $p=0.51$) (**Figure 6F**).

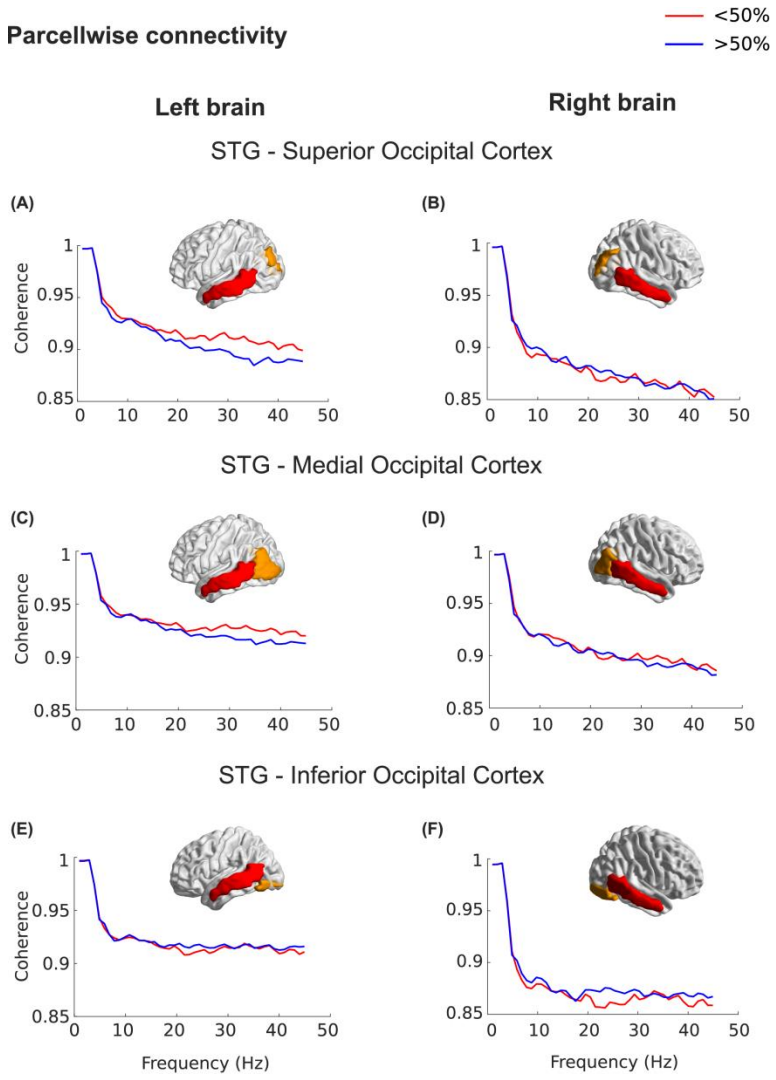

Figure 6 Pairwise connectivity between the parcels: Pairwise coherence between : (A) left Superior Temporal Gyrus (STG) and left Superior Occipital Cortex (SOC) (B) right STG and right SOC (C) left STG and left Medial Occipital Cortex (MOC) (D) right STG and right MOC (E) left STG and left Inferior Occipital Cortex (IOC) (F) right STG and right IOC. The brain images represent parcels between which the pairwise coherence is computed.

Discussion

An ongoing challenge in multisensory speech perception community is to accurately identify and characterize the neural mechanisms that govern the perceptual variability across individuals. Traditionally, studies have focused on identifying the neural correlates in terms of candidate brain regions or interactions among specific regions of interest that are responsible for the observed heterogeneity (Nath & Beauchamp, 2012). A more emerging understanding however, suggest the existence of large-scale networks of brain regions facilitating perceptual processing (Keil et al 2012; Beauchamp, 2015; Kumar et al 2017). Neuronal oscillations has been identified as a key marker of neuronal information processing in the relevant brain regions that needs to be fully explored to shape an individual's perceptual experience (Keil et al 2012; Kumar et al 2016, 2017; Keil & Senkowski, 2018). Robust oscillations observed from macroscopic recordings such as EEG/ MEG are an outcome of network interactions among local subpopulations of excitatory and inhibitory neurons (Wilson & Cowan, 1972; Deco et al., 2010; Becker et al., 2015). Empirically such interactions result in global coherence dynamics (Kumar et al., 2017). Our study demonstrates how distinct global coherence patterns correlate with inter-individual heterogeneity. Subsequently, using a computational model of interacting large-scale brain networks, we explain the plausible neural mechanisms that generate the coherence dynamics associated with the observed heterogeneity. Finally, we validate the plausible mechanism that emerged from the model about the connection parameters among interacting neural-subsystems using source-space functional connectivity analysis. Put together, we present an attractive mechanistic proposal that underlie the observed inter-individual variability in multisensory speech perception.

The two key conclusions from our study are – 1) susceptibility of individuals' McGurk effect is negatively correlated to their alpha band global coherence as a result of interactions among dynamical systems that individually operates in distinct time scales2) weakened functional associations between sensory specific areas, conceptualized as direct AV in our mechanistic model leads to the decrease in alpha band coherence in individuals with higher McGurk susceptibility.

Global coherence as the index of perceptual variability

Inter-individual differences observed in our study replicate (including reports from our group) and extend previous studies. 44% of our participants had more than 80% McGurk percept which lies within the range of 26% to 100% reported in previous studies (McGurk & Macdonald, 1976; MacDonald, et al., 2000; Benoit, et al., 2009; Nath & Beauchamp, 2012) (**Figure 2A**). Also, our mean McGurk percept (collapsed across participants) of 27% and 83% in rare and frequent perceivers respectively is within the literature range of 24% to 100% (McGurk & Macdonald, 1976; MacDonald, et al., 2000; Benoit, et al., 2009; Nath & Beauchamp, 2012; Strand et al., 2014) (**Figure 2B, C**). Hence, the behavioral results give confidence that the corresponding brain patterns will be of robust significance and general applicability. Our results show that the extent of de-synchronization of the cortical network in the alpha band indexes an individual's McGurk susceptibility (**Figure 3E, G, H**). This finding has two key elements. First, the inverse relationship between McGurk susceptibility and alpha band global coherence was consistent for McGurk stimulus and the congruent AV stimuli (/*ta*/ and /*ka*/) as well. This highlights that the propensity to perceive the McGurk illusion stems from inter-individual differences in perceptual categorization and not necessarily stimulus configurations. Second, it pinpoints that inter-individual variability defined as a functional state of the brain can be captured by exploring the dynamic repertoire of the underlying large-scale cortical network. The syllables /*ta*/ and /*ka*/ can be difficult to distinguish with visual cues alone, but acoustically are different. Therefore, coincidence of AV cues allows both the group of perceivers to reap the benefits of AV integration during congruent AV stimuli /*ta*/ and /*ka*/. However, the bilabial syllable /*pa*/ is very different visually from the alveolar syllable /*ta*/ and velar syllable /*ka*/. Hence, identification of the congruent AV syllable /*pa*/ does not necessarily require AV integration. Therefore, we do not see any significant correlation during congruent /*pa*/ stimulus.

Previous evidences accentuate the modulations in alpha band coherence to central executive processes (Klimesch, 1999; Sauseng et al., 2005), that are postulated to be involved in allocating working memory storage to phonological loop that maintains verbal information, and the visuo-spatial sketchpad that maintains transient visuo-spatial information (Baddeley, 1992). Such processes are involved in cross-modal perception that requires the integration of information from distributed neuronal assemblies. Taken together, communication via alpha coherence may

be the most plausible neuromarker of inter-group variability at the network level bearing the signature of integration.

Multisensory node operational at intermediate time-scale renders communication effective between sensory specific nodes operating at slow and fast time scales

Neural mass models that operate to explain mesoscopic and macroscopic features of dynamics in EEG/ MEG data offers an attractive tool to understand the underlying neural mechanisms (Silva et al., 1974; Jansen & Rit, 1995; David & Friston, 2003). The time scale of processing in our computational model is most disparate for the auditory and visual node, with auditory the fastest and visual the slowest (Rosen & Howell, 2011; Williams et al., 2004). Without the presence of an intermediate time-scale, only alpha coherence is sustained by the neural mass model within biologically relevant parameter regimes. On introduction of another neural mass operating at intermediate time-scale, synchronization in the gamma band emerges because higher dimensionality of the resultant dynamical system allows creation of another mode of communication exchange. Hence, our model suggests that emergence of gamma band coherence could be attributed to the communication between areas of auditory and visual cortices gated through multisensory areas such as STS. Our suggestion is in line with earlier observations of visual stimuli modulating auditory perception either directly resulting in alpha band coherence (Kayser et al., 2008) or indirectly via higher order regions resulting primarily in gamma band coherence (Maier et al., 2008; Kayser & Logothetis, 2009).

Drawing from the model, inter-individual differences primarily emerge from the differences in the A-V coupling. A stronger A-V coupling implies a lesser mediation via the multisensory node (stronger A-M and V-M) leading to weaker integration which is akin to rare perceivers. Conversely, lesser A-V coupling implies a larger involvement of the multisensory node (stronger A-M and V-M) in mediating the integration of the sensory inputs that is characteristic of frequent perceivers. Findings from our model corroborates with the earlier findings that pinpoint the significance of functional connectedness of the multisensory regions like STS to sensory specific, frontal and parietal regions in facilitating cross-modal perception (Keil et al., 2012).

Most importantly, we validated our predictions from the dynamical model to the empirical estimates of source-level functional connectivity. Pairwise connectivity between the parcel-level

time series (**Figure 6**) show increased connectivity between the auditory and visual parcels in rare than frequent perceivers. Interestingly, we observed this increase only in the left hemisphere which corroborates the earlier findings accentuating left laterality in multisensory speech perception (Beauchamp, 2010; Nath & Beauchamp, 2012; Keil et al., 2012).

The analysis pipeline (**Figure 1**), can be generalized easily to other studies of complex perceptual phenomena. For example, alpha and/or gamma coherences have been observed in AV perception studies involving speech phrases (Doesburg et al., 2008), natural scenes (Kayser et al., 2008) and also artificially generated AV looming signals (Maier et al., 2008). Modulations in AV interactions that explain differences in McGurk susceptibility in our study could also explain the increase in alpha phase consistency observed during natural AV scenes in rhesus monkeys (Kayser et al., 2008). Our model demonstrates that increase in the interaction between neural nodes operating at fast and slow time scales via a node operating at an intermediate time scale results in increased gamma and decreased alpha and beta band coherence. However, a slight tweak in the model topology elicits coherence modulations in varied frequency bands. A basic understanding that multifrequency coherent states of the network emerges from their difference in time scales can be used to explain a large repertoire of empirical observations.

Although our model of three interacting neural masses with different time-constants that generate band specific coherences can come across as a canonical model of neuronal network dynamics, certain limitations exist. Multi-parametric and unbounded nature of the parameter space results in myriads of dynamics including chaos which is non-biological (Stefanescu & Jirsa, 2008). Therefore, such models should not be used to directly fit the data using optimization techniques and should be limited to use as a phenomenological or minimalistic model in providing mechanistic insights into many findings (Fries, 2015; Engel et al., 2012), both normal and clinical.

Materials and Methods

Participants

Eighteen healthy right handed volunteers (8 females, mean age 24.9, SD = 2.8) gave written informed consent under an experimental protocol approved by the Institutional Human Ethics Committee of the National Brain Research Centre, Gurgaon which is in agreement with the Declaration of Helsinki.

Stimuli and behavioral task

A digital video of a native Hindi speaking male articulating the syllables /*pa*/, /*ka*/ and /*ta*/ was recorded and edited using – the audio editing software Audacity (www.audacityteam.org) and the video editing software Videopad Editor (www.nchsoftware.com). The duration of each video clip ranged from 1.5 to 1.7 seconds to include the neutral, mouth closed position and all the mouth movements of articulation to closing. The duration of auditory syllables in the videos ranged from 0.4 to 0.5 seconds. The stimuli (**Figure 7**) consisted of four kinds of videos: three congruent (auditory and visual matching) syllables (/*pa*/, /*ka*/, /*ta*/) and one McGurk/incongruent (auditory and visual mismatch) syllable (auditory /*pa*/ + visual /*ka*/) producing the McGurk percept of /*ta*/.

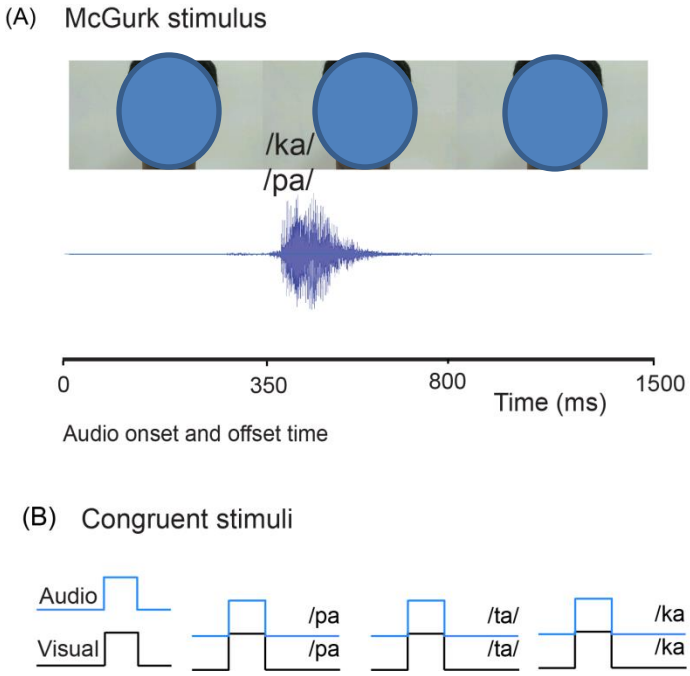

Figure 7 Stimuli: (A) Example trial with 3 video frames from McGurk stimulus (audio /*pa*/ + video /*ka*/) used in this experiment (top row), the audio trace of the syllable /*pa*/ presented simultaneously to the video (middle row) and the onset and offset time of the audio. (B)The congruent AV stimuli : each block represents a video with audio /*pa*/, /*ta*/ and /*ka*/ dubbed onto a video of a person articulating /*pa*/, /*ta*/ and /*ka*/ respectively.

The experiment contained five blocks – each block consisting 120 trials (30 trials of each video presented in random). Inter-stimulus intervals were pseudo-randomly varied between 1.2 seconds and 2.8 seconds to minimize expectancy effects. Using a forced choice task, on every trial, participant reported their percept by pressing a specified key on the keyboard corresponding to /*pa*/, /*ka*/, /*ta*/ or something else (others) while watching the videos.

EEG recording and preprocessing

Continuous EEG scans were acquired using a Neuroscan system (Synamps2, Compumedics, Inc.) with 64 Ag/AgCl scalp electrodes sintered on an elastic cap in a 10-20 montage. Individual electrode locations were registered using the Fastrak 3D digitizing system (Polhemus Inc.). Recordings were made against the centre (near Cz) reference electrode on the Neuroscan cap and digitized at a sampling rate of 1000 Hz. Channel impedances were monitored to be at values < 10kΩ.

Preprocessing and offline data analysis were performed using EEGLAB (Delorme & Makeig, 2004), Fieldtrip (Oostenveld et al. 2011) and custom made MATLAB scripts, Continuous data were high-passed at 0.1 Hz with finite impulse response (FIR) filters, low-passed at 80 Hz FIR and notch- filtered between 46-54 Hz to remove line noise (9th order 2-pass Butterworth filter). The noisy channels were removed and interpolated, following which the data was average re-referenced. For the data analysis, epochs of 0.8s post the onset of the sound were extracted and sorted based on the type of AV stimuli (congruent AV stimuli: /*ta*/, /*pa*/, /*ka*/ and incongruent McGurk stimulus) and the type of corresponding responses (/*ta*/, /*pa*/, /*ka*/ and 'others'). The sorted epochs were then baseline corrected by removing the temporal mean of the EEG signal 0.2s before the onset of the sound, on an epoch-by-epoch basis. Finally, epochs with amplitudes above or below ±75µV were removed to minimize contamination from ocular (eye blinks and movements) and muscle related artifacts.

Large-scale functional connectivity analysis

Neuronal synchronization was quantified using global coherence (Cimensar, et al. 2011). The metric quantifies the strength of covariation of neural oscillations at the global scale in specific frequency bands (Railo et al. 2011) that corresponds to specific functional state of the brain. We employed the Chronux (Mitra & Bokil, 2008) function CrossSpecMatc.m to obtain trial-wise

global coherence of the epochs sorted based on stimuli and responses. We considered 3 orthogonal discrete prolate spheroidal sequences (dpss), also known as Slepian tapers to restrict the leakage of spectral estimates into nearby frequency bins. The output variable 'Ctot' of the function yielded global coherence at frequency f .

The function initially multiplies the epochs with the specified number of Slepian tapers before performing the fast-fourier transform (FFT). The resulting FFT values are averaged and the cross-spectrum for all sensor combinations at frequency f are computed. The cross-spectral density between two sensors was computed from the tapered fourier transforms using the following equation

$$C_{ij} = conj(X_i(f).X_j(f)) \quad (1)$$

where, C_{ij} represents the cross-spectrum, X_i and X_j represent the tapered Fourier transforms from the sensors i and j. Subsequently, singular value decomposition (SVD) is applied on the cross-spectral density matrix for every frequency f which yields the following

$$D(f) = VCV^T \quad (2)$$

The diagonal matrix D comprises the values proportional to the variance explained by the orthogonal set of eigenvectors (V ,V^T). The global coherence $C_{Global}(f)$ at frequency bin f is subsequently computed by normalizing the largest eigenvalue (first entry of the $D(f)$ at frequency f on a trial-by-trial basis for each participant employing the following equation

$$C_{Global}(f) = \frac{D_1(f)}{\sum_{i=1}^{n} D_i(f)} \quad (3)$$

We initially analyzed if changes in global coherence values at specific frequency bands (alpha: 8-13Hz, beta: 14-30Hz, gamma: 31-45Hz) correlated with the participants' susceptibility of McGurk perception. Participant-wise mean of the global coherence in specific frequency bands were computed and were statistically analyzed using Spearman rank correlation and t-tests.

In order to extract the dynamics of the global coherence that supported cross-modal percept, we sorted our participants based on their percentage susceptibility of McGurk effect into two groups - rare perceivers (<50% /*ta*/ percept) and frequent perceivers (>50% /*ta*/ percept). Subsequently, the global coherence computed on a trial-by-trial basis was sorted based on the perceptual categories (/*ta*/ and /*pa*/) and averaged over all the participants and compared in each group explicitly employing cluster based permutation tests (Maris et al., 2007; Kumar et al., 2016).

Architecture of large scale dynamical model of perception

To account the neuronal interactions that could facilitate changes in global coherence, we constructed a large-scale dynamical model. Striking a balance between biological realism and model parsimony, we proposed a neural-mass model comprising three nodes representing the auditory, visual and the multisensory areas (**Figure 8A**). We followed closely a previously established practice and convention in computational modeling by treating each cortical region as an individual node comprising excitatory and inhibitory population of Hindmarsh Rose (HR) neurons (Stefanescu & Jirsa, 2008). Rationally, we incorporate the following factors to reflect the biological realism in the proposed model architecture -

1. Concurring with previous evidences, auditory node was assumed to be most sensitive to ambient temporal fluctuations operating with a fast time-scale (Rosen & Howell, 2011), Visual node was assumed to be slowest in terms of sensitivity (Williams et al., 2004) and the multisensory node was assumed to operate at an intermediate time-scale.
2. Inspired by the anatomical evidences, in our model, inputs from visual node were directed to the auditory cortex in two ways: i) direct influence in a feedforward manner (Falchier et al., 2002; Rockland & Ojima, 2003; Wallace et al., 2004) and ii) in feedback manner via the multisensory association node (Bizley & King, 2012).
3. Excitatory and inhibitory afferents on the spatially extended and geometrically aligned pyramidal neurons result in post-synaptic potentials (Kirschstein & Köhling, 2009), These communication emerge as EEG patterns. Hence, we used a population of excitatory and inhibitory neurons in each node (**Figure 8B**). Following the approach used by Stefanescu and Jirsa (Stefanescu & Jirsa, 2008), we employed a total of 150 excitatory ($N_E = 150$) and 50 inhibitory ($N_I = 50$) HR neurons, maintaining a ratio of 3:1. Importantly, inhibitory neurons

within an individual node were not coupled directly with other inhibitory neurons based on the logic that these connections in microcircuits are typically sparse in nature (Wilson & Cowan, 1972; Stefanescu & Jirsa, 2008).

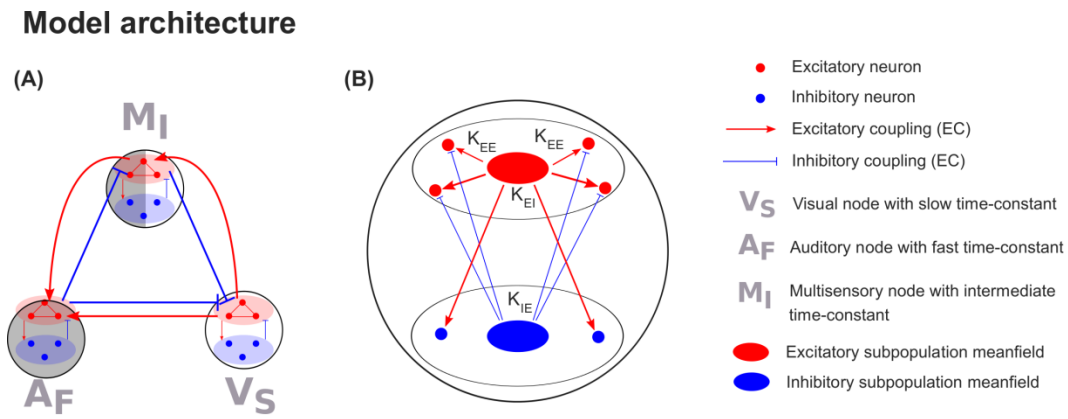

Figure 8 Model architecture: (A) Representation of the model comprising three nodes signifying auditory (fast time-constant), visual (slow time-constant) and higher order multisensory regions (intermediate time-constant). Excitatory influences between the nodes are balanced by their inhibitory counterpart. (B) Representation of each node comprising of network of 100 Hindmarsh-Rose excitatory and 50 inhibitory neurons. Each neuron can exhibit isolated spiking, periodic spiking and bursting behavior.

Incorporating the aforementioned factors, we defined a dynamic mean field comprising three sets of ordinary differential equations for each excitatory and inhibitory HR neurons. The three variables $\hat{x}$, $\hat{y}$ and $\hat{z}$ account for the membrane potential dynamics, fast and slow gating currents respectively. Thus, the entire network can be represented as a network of coupled non-linear differential equations containing -

Excitatory Subpopulation

$$\tau_L \frac{dx_{n_E}^L}{dt} = y_{n_E}^L - a x_{n_E}^{L^3} + b x_{n_E}^{L^2} - z_{n_E}^L + K_{EE}(\mathrm{E}(x_{n_E}^L) - x_{n_E}^L) - K_{IE}(\mathrm{E}(x_{n_I}^L) - x_{n_E}^L) + I_{n_E}^L + \sum_{M=1}^{3} W_{ML}\mathrm{E}(x_{n_E}^M) + \square\,(0, \varepsilon dt)$$

$$\tau_L \frac{dy_{n_E}^L}{dt} = c - d x_{n_E}^{L^2} - y_{n_E}^L$$

$$\tau_L \frac{dz_{n_E}^L}{dt} = r(s(x_{n_E}^L - x_0) - z_{n_E}^L); n_E = 1, \ldots, N_E; L = 1(A), 2(M) \,\&\, 3(V)$$

Inhibitory Subpopulation (4)

$$\tau_L \frac{dx_{n_I}^L}{dt} = y_{n_I}^L - ax_{n_I}^{L^3} + bx_{n_I}^{L^2} - z_{n_I}^L + K_{EI}(\mathrm{E}(x_{n_E}^L) - x_{n_I}^L) + I_{n_I}^L$$

$$\tau_L \frac{dy_{n_I}^L}{dt} = c - dx_{n_I}^{L^2} - y_{n_I}^L$$

$$\tau_L \frac{dz_{n_I}^L}{dt} = r(s(x_{n_I}^L - x_0) - z_{n_I}^L); n_I = 1,...,N_I; L = 1(A), 2(M) \,\&\, 3(V)$$

where L: A, V and M represent auditory, visual and multisensory nodes respectively. The nodes were driven by a noise of normal distribution $\square(0, \varepsilon dt)$, where ε is $1e-1$. Auditory node had the fastest ($\tau_A \sim 0.05ms$) and visual node had the slowest time-constant ($\tau_V \sim 2.5ms$). Time-constant of the multisensory node was chosen to be in between the two ($\tau_M \sim 1ms$) as it integrates information from both the modalities. The mean activity of excitatory neurons in a given node ($\mathrm{E}(x_{n_E}) = \frac{1}{N_E}\sum_{n_E=1}^{N_E} x_{n_E}$) influencing the neuronal activity of other nodes was governed by coupling parameters: W_{AV} (auditory-visual coupling), W_{AM} (auditory-multisensory coupling) and W_{VM} (visual-multisensory coupling). Positive and negative values of the coupling parameters reflect excitatory and inhibitory coupling respectively. Inhibitory couplings were chosen to maintain a balance with excitation. For instance, visual node's excitatory coupling of $+W_{AV}$ on auditory node was balanced with inhibitory coupling of the same strength ($-W_{AV}$) from the auditory node. Also, in such a configuration, visual node is being the source of excitation, is referred as the source whereas auditory node is referred as the sink since all excitatory couplings are directed towards it. The multisensory node in such configuration behaves as both source and sink.

We place each individual neuron in a dynamical regime where both spiking and bursting behavior is possible depending on the external input current (I) that enters the neuron when other parameters are held constant at the following values:

$a = 1; b = 3; c = 1; d = 5; s = 4; r = 0.006; x_0 = -1.6$. (Stefanescu & Jirsa, 2008).

The coupling between neurons within a node was linear and its strength was governed by the following parameters: K_{EE} for excitatory-excitatory coupling, K_{EI} for excitatory-inhibitory coupling and K_{IE} for inhibitory-excitatory coupling. Within a node, the relation between K_{EE} and K_{IE} was captured by the ratio $n = \frac{K_{IE}}{K_{EE}}$. Electrophysiological evidences indicate enhanced oscillatory power in delta (1-4 Hz) and alpha (8-12 Hz) bands during rest (Gold et al., 2006). To emulate the characteristics of the large-scale network during rest, we chose the value of the ratio, $n = 3.39$ where the average oscillatory activity of the nodes in a disconnected network i.e. in the absence of stimulus ($\mu(I_{A,V,M}) = 0.1$; baseline) was higher in delta and alpha bands.

The external currents to both the excitatory and inhibitory subpopulations were drawn from a Gaussian distribution where μ and σ represent the mean and standard-deviation. As the input stimulus relays to auditory, visual and multisensory regions via thalamus, we interpret lateral geniculate nucleus (LGN) and medial geniculate nucleus (MGN) to be the source of external current (I_A, I_V and I_M) – a pulse of 450 ms in the nodes when the model was simulated for 1 second. In rhesus monkey, the projections of MGN to multisensory areas like STS were found to be sparse (Yeterian & Pandya, 1989). Therefore, we choose lower mean value of external current to the multisensory node ($\mu(I_M) = 0.85$) in comparison to visual ($\mu(I_V) = 2.8$) and auditory ($\mu(I_V) = 2.8$) node.

We hypothesized that variability in global coherence patterns to emerge from differences in the coupling between the sensory specific and multisensory brain regions operating at fast, slow and intermediate time scales respectively. Therefore, we sought to explore the global coherence while varying the coupling strength among the nodes in our model.

Table 2: Description of the model parameters and their corresponding values used in the model.

Parameter	Value	Description of parameters
$a,\ b,\ c,\ d$	$1, 3, 1, 5$	Constants for faster variables x & y
r	0.006	Lower value of r is responsible for slower time-scale of z
s	4	Constant affecting slower variable z
x_0	-1.6	$(x_0, y_0, 0)$ is a stable equilibrium point of Hindmarsh-Rose model.
$N_E,\ N_I$	$150,\ 50$	Number of excitatory and inhibitory neurons in each node
μ, σ	$2.8,\ 0.4$	Mean and dispersion of input current in each node
I_{n_E}, I_{n_I}	Computed from mu and sigma	Input current for excitatory and inhibitory neurons in each node
τ_A, τ_V, τ_M	$0.05,\ 2.5,\ 1$ in milliseconds	Time-scales for auditory, visual and multisensory nodes
ε	0.1	Constant affecting the dispersion of noise
Within nodes connectivity		
K_{EE}	0.5	Coupling between excitatory neurons
K_{EI}	0.5	Excitatory to inhibitory coupling
n	3.39	K_{IE} to K_{EE} ratio
K_{IE}	Computed from n and K_{EE}	Inhibitory to excitatory coupling
Between nodes connectivity		
W_{AV}, W_{AM}, W_{VM}	Explored in the range 0 to 1 (or -1 to 0)	
State Variables		
x_{n_E}, x_{n_I}	Membrane potentials for excitatory and inhibitory subpopulation	
y_{n_E}, y_{n_I}	Spiking variables for excitatory and inhibitory subpopulation	
z_{n_E}, z_{n_I}	Bursting variables for excitatory and inhibitory subpopulation	

Source-space connectivity

To validate the inferences gathered from our model, we turned to the empirical data again and undertook source-space connectivity analysis (see **Figure 1**). We employed dynamic imaging of coherent sources (DICS) (Gross et al., 2001)- a frequency domain adaptive spatial filtering algorithm - to identify the sources of global coherence in specific frequency bands. This algorithm has proven to be particularly powerful in localizing oscillatory sources of cortical activity with well-established hypothesis (Halder et al., 2019) . Customized MATLAB codes employing Fieldtrip toolbox were used. Using ft_prepare_leadfeild.m and employing the Boundary Element Method (BEM), we generated the leadfield matrix for the Colin27 brain template. The leadfield matrix corresponds to the tissue and geometrical properties of the brain represented as discrete grids or voxels. Then, we employed ft_freqanalysis.m to evaluate the crossspectral matrices of the epochs pooled over participants in each group (rare and frequent). Leadfield matrix and the cross-spectral matrices were used to compute the spatial filters that regulate the amplitude of brain electrical activity passing from a specific location while attenuating activity originating at other locations. The distribution of the output amplitude of the spatial filters provides the metric for source localization. Subsequently, employing ft_sourceanalysis.m we computed source power at each voxel defined by our leadfield matrix.

To reduce the dimensionality in our source-space connectivity analysis, we adopted a parcellation scheme before generating source-time series. We combined the source estimates of the voxels using the labeling according to Automated Anatomical Labelling (AAL) atlas (Tzourio-Mazoyer et al., 2002). Then, for reconstructing the parcel-wise time series, we projected single trial epoched time series to the source-space by multiplying them with spatial filter of the respective parcel. Subsequently, we computed the coherence between relevant parcels for rare and frequent perceivers explicitly.

Finally, to compare the differences in pairwise coherence between rare and frequent perceivers, we performed permutation test. Initially, for each relevant parcel, from the trials pooled over participants in each group (rare and frequent), 500 trails were randomly picked to form two sets of random partition. Subsequently, pairwise coherence between the parcels (**Figure 6**) were computed on a trail-by-trail basis and averaged for rare and frequent perceivers separately.

The aforementioned steps were repeated 1000 times to generate a distribution of pairwise coherence values for frequent and rare perceivers. Finally, the distribution of pairwise coherence values compared between rare and frequent perceivers using *Student's t-test.*

Acknowledgements

The study was supported by NBRC Core funds and by grants Ramalingaswami fellowship, (BT/RLF/Re-entry/31/2011) and Innovative Young Bio-technologist Award (IYBA), (BT/07/IYBA/2013) from the Department of Biotechnology (DBT), Ministry of Science and Technology, Government of India to AB. AB also acknowledges thesupport of Centre of Excellence in Epilepsy and MEG (BT/01/COE/09/08/2011) from DBT. DR was supported by the Ramalingaswami fellowship (BT/RLF/Re-entry/07/2014) from DBT.

References

Baddeley, A. (1992). Working memory. *Science*, *255*(5044), 556–559. http://doi.org/10.1126/science.1736359

Beauchamp, M. S. (2010). fMRI-guided TMS reveals that the STS is a Cortical Locus of the McGurk Effect. *Journal of Neuroscience*, *30*(7), 2414–2417. http://doi.org/10.1523/JNEUROSCI.4865-09.2010.fMRI-guided

Beauchamp, M. S. (2015). The social mysteries of the superior temporal sulcus. *Trends in Cognitive Sciences*, *19*(9), 489–490. http://doi.org/10.1016/j.tics.2015.07.002

Becker, R., Knock, S., Ritter, P., & Jirsa, V. (2015). Relating Alpha Power and Phase to Population Firing and Hemodynamic Activity Using a Thalamo-cortical Neural Mass Model. *PLoS Computational Biology*, *11*(9), e1004352. http://doi.org/10.1371/journal.pcbi.1004352

Benoit, M. M., Raij, T., Lin, F.-H., Jääskeläinen, I. P., & Stufflebeam, S. (2009). Primary and multisensory cortical activity is correlated with audiovisual percepts. *Human Brain Mapping*, *31*(4), NA-NA. http://doi.org/10.1002/hbm.20884

Bizley, J. K., & King, A. J. (2012). *What Can Multisensory Processing Tell Us about the Functional Organization of Auditory Cortex? The Neural Bases of Multisensory Processes*. CRC Press/Taylor & Francis. Retrieved from http://www.ncbi.nlm.nih.gov/pubmed/22593889

Bressler, S. L. (1995). Large-scale cortical networks and cognition. *Brain Research Reviews*, *20*(3), 288–304. http://doi.org/10.1016/0165-0173(94)00016-I

Bressler, S. L., & Kelso, J. A. S. (2001). Cortical coordination dynamics and cognition. *Trends in Cognitive Sciences*, *5*(1), 26–36. http://doi.org/10.1016/S1364-6613(00)01564-3

Bressler, S. L., & Menon, V. (2010). Large-scale brain networks in cognition: emerging methods and principles. *Trends in Cognitive Sciences*, *14*(6), 277–290. http://doi.org/10.1016/j.tics.2010.04.004

Cuppini, C., Shams, L., Magosso, E., & Ursino, M. (2017). A biologically inspired neurocomputational model for audiovisual integration and causal inference. *European Journal of Neuroscience*, *46*(9), 2481–2498. http://doi.org/10.1111/ejn.13725

David, O., & Friston, K. J. (2003). A neural mass model for MEG/EEG: coupling and neuronal dynamics. *NeuroImage*, *20*(3), 1743–55. Retrieved from http://www.ncbi.nlm.nih.gov/pubmed/14642484

Deco, G., Pérez-Sanagustín, M., de Lafuente, V., & Romo, R. (2007). Perceptual detection as a dynamical bistability phenomenon: a neurocomputational correlate of sensation. *Proceedings of the National Academy of Sciences of the United States of America*, *104*(50), 20073–7. http://doi.org/10.1073/pnas.0709794104

Deco, G., Rolls, E. T., & Romo, R. (2010). Synaptic dynamics and decision making.

Proceedings of the National Academy of Sciences of the United States of America, *107*(16), 7545–9. http://doi.org/10.1073/pnas.1002333107

Delorme, A., & Makeig, S. (2004). EEGLAB: an open source toolbox for analysis of single-trial EEG dynamics including independent component analysis. *Journal of Neuroscience Methods*, *134*(1), 9–21. http://doi.org/10.1016/j.jneumeth.2003.10.009

Doesburg, S. M., Emberson, L. L., Rahi, A., Cameron, D., & Ward, L. M. (2008). Asynchrony from synchrony: long-range gamma-band neural synchrony accompanies perception of audiovisual speech asynchrony. *Experimental Brain Research*, *185*(1), 11–20. http://doi.org/10.1007/s00221-007-1127-5

Engel, A. K., Senkowski, D., & Schneider, T. R. (2012). *Multisensory Integration through Neural Coherence*. *The Neural Bases of Multisensory Processes*. CRC Press/Taylor & Francis. Retrieved from http://www.ncbi.nlm.nih.gov/pubmed/22593880

Falchier, A., Clavagnier, S., Barone, P., & Kennedy, H. (2002). Anatomical evidence of multimodal integration in primate striate cortex. *The Journal of Neuroscience : The Official Journal of the Society for Neuroscience*, *22*(13), 5749–59. http://doi.org/20026562

Fries, P. (2015). Rhythms for Cognition: Communication through Coherence. *Neuron*, *88*(1), 220–235. http://doi.org/10.1016/j.neuron.2015.09.034

Gold, C., Henze, D. A., Koch, C., & Buzsáki, G. (2006). On the Origin of the Extracellular Action Potential Waveform: A Modeling Study. *Journal of Neurophysiology*, *95*(5), 3113–3128. http://doi.org/10.1152/jn.00979.2005

Gross, J., Kujala, J., Hamalainen, M., Timmermann, L., Schnitzler, A., & Salmelin, R. (2001). Dynamic imaging of coherent sources: Studying neural interactions in the human brain. *Proceedings of the National Academy of Sciences of the United States of America*, *98*(2), 694–9. http://doi.org/10.1073/pnas.98.2.694

Halder, T., Talwar, S., Jaiswal, A. K., & Banerjee, A. (2019). Quantitative Evaluation in Estimating Sources Underlying Brain Oscillations Using Current Source Density Methods and Beamformer Approaches. *ENeuro*, *6*(4), ENEURO.0170-19.2019. http://doi.org/10.1523/ENEURO.0170-19.2019

Haxby, J. V., Hoffman, E. A., & Gobbini, M. I. (2000). The distributed human neural system for face perception. *Trends in Cognitive Sciences*, *4*(6), 223–233. http://doi.org/10.1016/S1364-6613(00)01482-0

Hindmarsh, J. L., & Rose, R. M. (1984). A model of neuronal bursting using three coupled first order differential equations. *Proceedings of the Royal Society of London. Series B, Biological Sciences*, *221*(1222), 87–102. Retrieved from http://www.ncbi.nlm.nih.gov/pubmed/6144106

Jansen, B. H., & Rit, V. G. (1995). Electroencephalogram and visual evoked potential generation in a mathematical model of coupled cortical columns. *Biological Cybernetics*, *73*(4), 357–66. Retrieved from http://www.ncbi.nlm.nih.gov/pubmed/7578475

Kayser, C., & Logothetis, N. K. (2009). Directed interactions between auditory and superior temporal cortices and their role in sensory integration. *Frontiers in Integrative Neuroscience*, *3*, 7. http://doi.org/10.3389/neuro.07.007.2009

Kayser, C., Petkov, C. I., & Logothetis, N. K. (2008). Visual Modulation of Neurons in Auditory Cortex. *Cerebral Cortex*, *18*(7), 1560–1574. http://doi.org/10.1093/cercor/bhm187

Keil, J., Muller, N., Ihssen, N., & Weisz, N. (2012). On the Variability of the McGurk Effect: Audiovisual Integration Depends on Prestimulus Brain States. *Cerebral Cortex*, *22*(1), 221–231. http://doi.org/10.1093/cercor/bhr125

Keil, J., & Senkowski, D. (2018). Neural Oscillations Orchestrate Multisensory Processing. *The Neuroscientist*, 107385841875535. http://doi.org/10.1177/1073858418755352

Kirschstein, T., & Köhling, R. (2009). What is the Source of the EEG? *Clinical EEG and Neuroscience*, *40*(3), 146–149. http://doi.org/10.1177/155005940904000305

Klimesch, W. (1999). EEG alpha and theta oscillations reflect cognitive and memory performance: a review and analysis. *Brain Research Reviews*, *29*, 169–195.

Körding, K. P., Beierholm, U., Ma, W. J., Quartz, S., Tenenbaum, J. B., & Shams, L. (2007). Causal Inference in Multisensory Perception. *PLoS ONE*, *2*(9), e943. http://doi.org/10.1371/journal.pone.0000943

Kumar, G. V., Halder, T., Jaiswal, A. K., Mukherjee, A., Roy, D., & Banerjee, A. (2016). Large Scale Functional Brain Networks Underlying Temporal Integration of Audio-Visual Speech Perception: An EEG Study. *Frontiers in Psychology*, *7*, 1558. http://doi.org/10.3389/fpsyg.2016.01558

Kumar, G. V., Kumar, N., Roy, D., & Banerjee, A. (2017). Segregation and Integration of Cortical Information Processing Underlying Cross-Modal Perception. *Multisensory Research*, (Special issue), 1–20. http://doi.org/10.1163/22134808-00002574

Lopes da Silva, F. H., Hoeks, A., Smits, H., & Zetterberg, L. H. (1974). Model of brain rhythmic activity. The alpha-rhythm of the thalamus. *Kybernetik*, *15*(1), 27–37. Retrieved from http://www.ncbi.nlm.nih.gov/pubmed/4853232

Ma, W. J., Beck, J. M., & Pouget, A. (2008). Spiking networks for Bayesian inference and choice. *Current Opinion in Neurobiology*, *18*(2), 217–222. http://doi.org/10.1016/j.conb.2008.07.004

MacDonald, J., Andersen, S., & Bachmann, T. (2000). Hearing by Eye: How Much Spatial Degradation can Be Tolerated? *Perception*, *29*(10), 1155–1168. http://doi.org/10.1068/p3020

Magosso, E., Cuppini, C., & Ursino, M. (2012). A Neural Network Model of Ventriloquism Effect and Aftereffect. *PLoS ONE*, *7*(8), e42503. http://doi.org/10.1371/journal.pone.0042503

Maier, J. X., Chandrasekaran, C., & Ghazanfar, A. A. (2008). Integration of Bimodal Looming

Signals through Neuronal Coherence in the Temporal Lobe. *Current Biology*, *18*(13), 963–968. http://doi.org/10.1016/j.cub.2008.05.043

Maris, E., Schoffelen, J.-M., & Fries, P. (2007). Nonparametric statistical testing of coherence differences. *Journal of Neuroscience Methods*, *163*(1), 161–75. http://doi.org/10.1016/j.jneumeth.2007.02.011

McGurk, H., & Macdonald, J. (1976). Hearing lips and seeing voices. *Nature*, *264*, 691–811. http://doi.org/10.1038/264746a0

Mitra, P., & Bokil, H. (2008). *Observed brain dynamics*. Oxford Univ Press, New York.

Nath, A. R., & Beauchamp, M. S. (2011). Dynamic changes in superior temporal sulcus connectivity during perception of noisy audiovisual speech. *The Journal of Neuroscience : The Official Journal of the Society for Neuroscience*, *31*(5), 1704–14. http://doi.org/10.1523/JNEUROSCI.4853-10.2011

Nath, A. R., & Beauchamp, M. S. (2012). A neural basis for interindividual differences in the McGurk effect, a multisensory speech illusion. *NeuroImage*, *59*(1), 781–787. http://doi.org/10.1016/j.neuroimage.2011.07.024

Onojima, T., Goto, T., Mizuhara, H., & Aoyagi, T. (2018). A dynamical systems approach for estimating phase interactions between rhythms of different frequencies from experimental data. *PLOS Computational Biology*, *14*(1), e1005928. http://doi.org/10.1371/journal.pcbi.1005928

Oostenveld, R., Fries, P., Maris, E., & Schoffelen, J.-M. (2011). FieldTrip: Open source software for advanced analysis of MEG, EEG, and invasive electrophysiological data. *Computational Intelligence and Neuroscience*, *2011*, 156869. http://doi.org/10.1155/2011/156869

Puce, A., & Perrett, D. (2003). Electrophysiology and brain imaging of biological motion. *Philosophical Transactions of the Royal Society of London. Series B: Biological Sciences*, *358*(1431), 435–445. http://doi.org/10.1098/rstb.2002.1221

Railo, H., Koivisto, M., & Revonsuo, A. (2011). Tracking the processes behind conscious perception: A review of event-related potential correlates of visual consciousness. *Consciousness and Cognition*, *20*(3), 972–983. http://doi.org/10.1016/j.concog.2011.03.019

Rockland, K. S., & Ojima, H. (2003). Multisensory convergence in calcarine visual areas in macaque monkey. *International Journal of Psychophysiology : Official Journal of the International Organization of Psychophysiology*, *50*(1–2), 19–26. Retrieved from http://www.ncbi.nlm.nih.gov/pubmed/14511833

Rosen, S., & Howell, P. (2011). *Signals and systems for speech and hearing / S. Rosen and P. Howell - Details - Trove*. Retrieved from https://trove.nla.gov.au/work/6339833

Sauseng, P., Klimesch, W., Schabus, M., & Doppelmayr, M. (2005). Fronto-parietal EEG coherence in theta and upper alpha reflect central executive functions of working memory. *International Journal of Psychophysiology*, *57*(2), 97–103. http://doi.org/10.1016/j.ijpsycho.2005.03.018

Saxe, R. (2006). Uniquely human social cognition. *Current Opinion in Neurobiology*, *16*(2), 235–239. http://doi.org/10.1016/J.CONB.2006.03.001

Spiegler, A., Knösche, T. R., Schwab, K., Haueisen, J., & Atay, F. M. (2011). Modeling Brain Resonance Phenomena Using a Neural Mass Model. *PLoS Computational Biology*, *7*(12), e1002298. http://doi.org/10.1371/journal.pcbi.1002298

Stefanescu, R. A., & Jirsa, V. K. (2008). A Low Dimensional Description of Globally Coupled Heterogeneous Neural Networks of Excitatory and Inhibitory Neurons. *PLoS Computational Biology*, *4*(11), e1000219. http://doi.org/10.1371/journal.pcbi.1000219

Strand, J., Cooperman, A., Rowe, J., & Simenstad, A. (2014). Individual Differences in Susceptibility to the McGurk Effect: Links With Lipreading and Detecting Audiovisual Incongruity. *Journal of Speech, Language, and Hearing Research*, *57*(6), 2322–2331. http://doi.org/10.1044/2014_JSLHR-H-14-0059

Thakur, B., Mukherjee, A., Sen, A., & Banerjee, A. (2016). A dynamical framework to relate perceptual variability with multisensory information processing. *Scientific Reports*, *6*(1), 31280. http://doi.org/10.1038/srep31280

Tzourio-Mazoyer, N., Landeau, B., Papathanassiou, D., Crivello, F., Etard, O., Delcroix, N., … Joliot, M. (2002). Automated Anatomical Labeling of Activations in SPM Using a Macroscopic Anatomical Parcellation of the MNI MRI Single-Subject Brain. *NeuroImage*, *15*(1), 273–289. http://doi.org/10.1006/NIMG.2001.0978

Ursino, M., Crisafulli, A., di Pellegrino, G., Magosso, E., & Cuppini, C. (2017). Development of a Bayesian Estimator for Audio-Visual Integration: A Neurocomputational Study. *Frontiers in Computational Neuroscience*, *11*, 89. http://doi.org/10.3389/fncom.2017.00089

Varela, F., Lachaux, J.-P., Rodriguez, E., & Martinerie, J. (2001). The brainweb: Phase synchronization and large-scale integration. *Nature Reviews Neuroscience*, *2*(4), 229–239. http://doi.org/10.1038/35067550

Wallace, M. T., Ramachandran, R., & Stein, B. E. (2004). A revised view of sensory cortical parcellation. *Proceedings of the National Academy of Sciences of the United States of America*, *101*(7), 2167–72. http://doi.org/10.1073/pnas.0305697101

Williams, P. E., Mechler, F., Gordon, J., Shapley, R., & Hawken, M. J. (2004). Entrainment to Video Displays in Primary Visual Cortex of Macaque and Humans. *Journal of Neuroscience*, *24*(38), 8278–8288. http://doi.org/10.1523/JNEUROSCI.2716-04.2004

Wilson, H. R., & Cowan, J. D. (1972). Excitatory and Inhibitory Interactions in Localized Populations of Model Neurons. *Biophysical Journal*, *12*(1), 1–24. http://doi.org/10.1016/S0006-3495(72)86068-5

Yeterian, E. H., & Pandya, D. N. (1989). Thalamic connections of the cortex of the superior temporal sulcus in the rhesus monkey. *The Journal of Comparative Neurology*, *282*(1), 80–97. http://doi.org/10.1002/cne.902820107